Chapter 5: Observations: Oceanic Climate Change and Sea Level
Figures

Coordinating Lead Authors: Nathaniel Bindoff (Australia), Jürgen Willebrand (Germany)

Lead Authors: Vincenzo Artale (Italy), Anny Cazenave (France), Jonathan Gregory (UK), Sergey Gulev (Russia), Kimio Hanawa (Japan), Corinne Le Quéré (Germany), Sydney Levitus (USA), Yukihiro Nojiri (Japan), C.K. Shum (USA), Lynne Talley (USA), Alakkat Unnikrishnan (India)

Contributing Authors: J. Antonov (USA, Russia), N. Bates (Bermuda, UK, Canada), T.Boyer (USA), D. Chambers (USA), B. Chao (USA), J.A. Church (Australia), R. Curry (USA), S. Emerson (USA), R. Feely (USA), H. Garcia (USA), M. González-Dávila (Spain), N. Gruber (USA, Switzerland), S. Josey (UK), T. Joyce (USA), K. Kim (Korea), B. King (UK), A. Körtzinger (Germany), K. Lambeck (Australia), K. Laval (France), N. Lefèvre (France), E. Leuliette (USA), R. Marsh (UK), C. Mauritzen (Norway), M. McPhaden (USA), C. Millot (France), C. Milly (USA), R. Molinari (USA), S. Nerem (USA), T. Ono (Japan), M. Pahlow (Canada), T. Peng (USA), A. Proshutinsky (USA), D. Quadfasel (Germany), B. Qiu (USA), S. Rahmstorf (Germany), S. Rintoul (Australia), M. Rixen (NATO, Belgium), P. Rizzoli (USA, Italy), C. Sabine (USA), D. Sahagian (USA), F. Schott (Germany), Y. Song (USA), D. Stammer (Germany), T. Suga (Japan), C. Sweeney (USA), M. Tamisiea (USA), M. Tsimplis (UK, Greece), R. Wanninkhof (USA), J. Willis (USA), A.P. Wong (USA, Australia), P. Woodworth (UK), I. Yashayaev (Canada), I. Yasuda (Japan)

Review Editors: Laurent Labeyrie (France), David Wratt (New Zealand)

Date of Draft: 27 October 2006

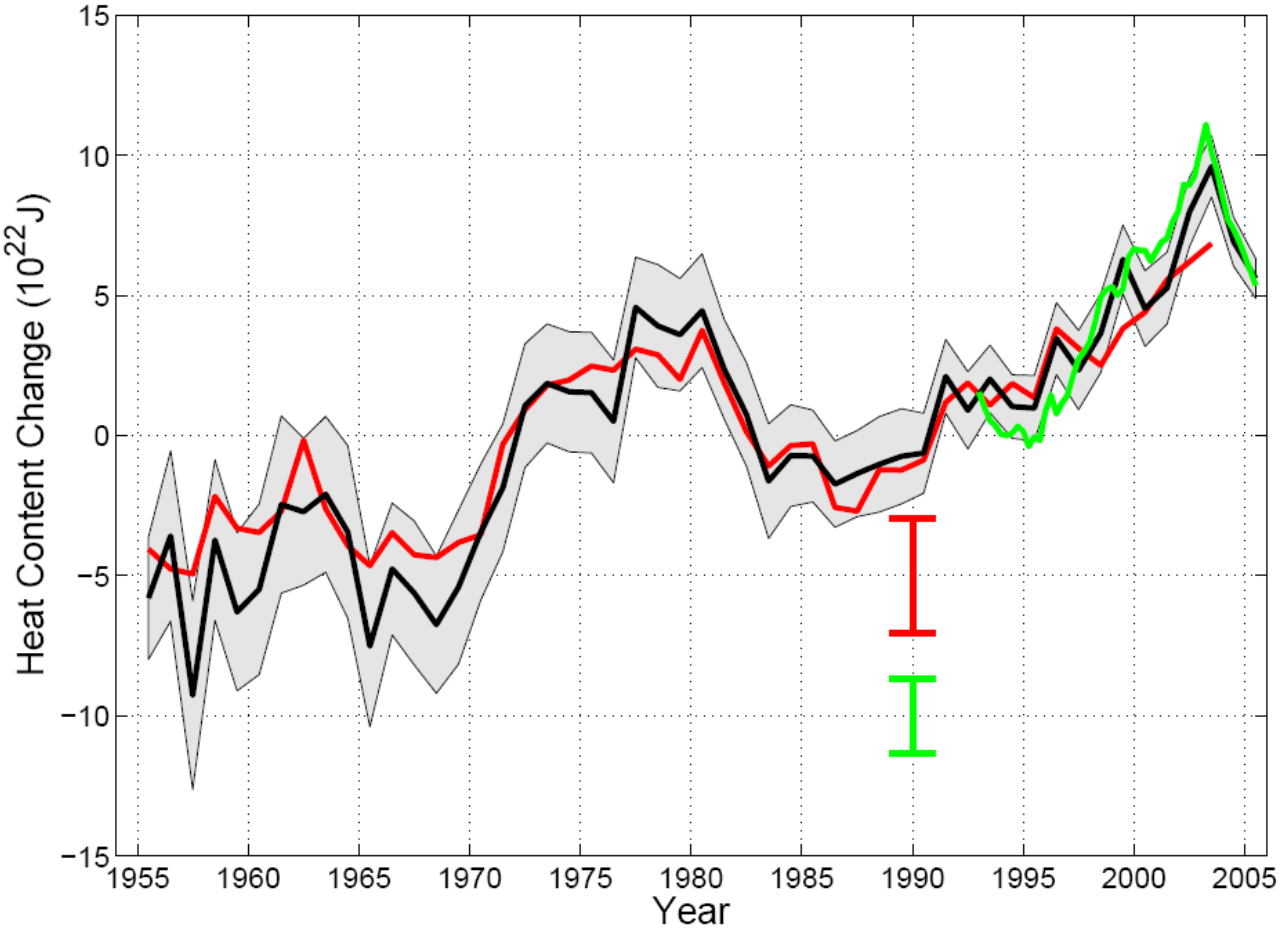

Figure 5.1. Time series of global, yearly ocean heat content (10^{22} J) for the 0–700 m layer. The black curve is updated from Levitus et al. (2005a), with the shading representing the 90% confidence interval. The red and green curves are updates of the analyses by Ishii et al. (2006) and Willis et al. (2004, over 0–750 m), with the error bars denoting 90% confidence interval. The black and red curves denote the deviation from their 1961–1990 average and the shorter green curve the deviation from the average of the black curve for the period 1993–2003.

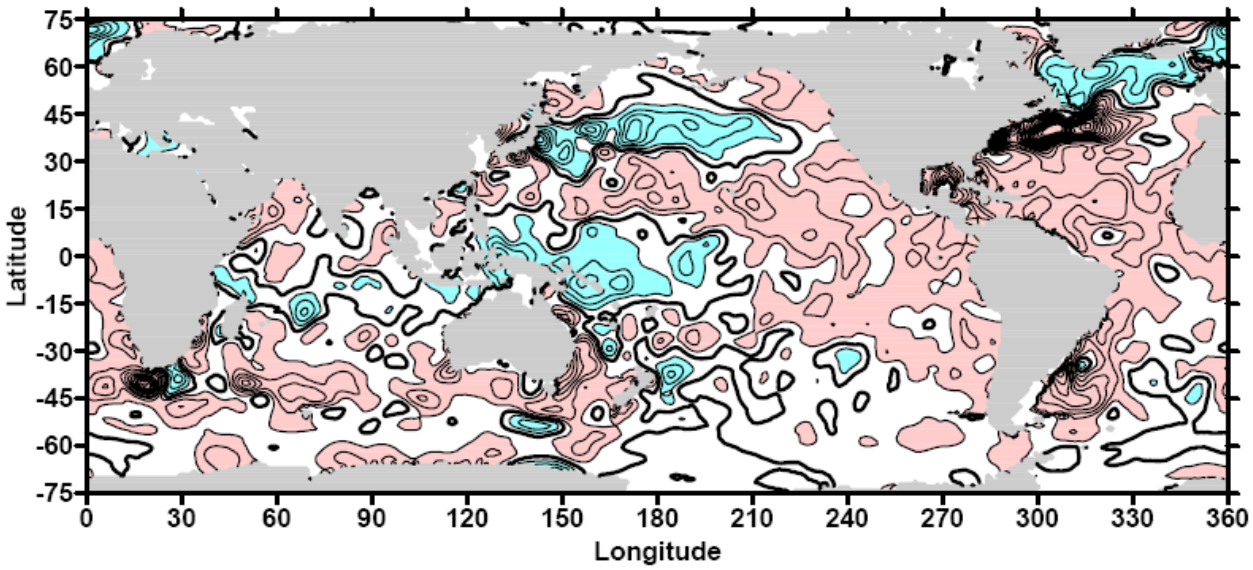

Figure 5.2. Linear trends (1955–2003) of change in ocean heat content per unit surface area for the 0–700 m layer, based on the work of Levitus et al. (2005a), in units of W m^{-2}. The linear trend is computed at each grid point using a least squares fit to the time series at each gridpoint. Contour interval is 0.25 W m^{-2}. Red shading indicates values equal or greater than 0.25 W m^{-2} and blue shading indicates values equal or less than –0.25 W m^{-2}.

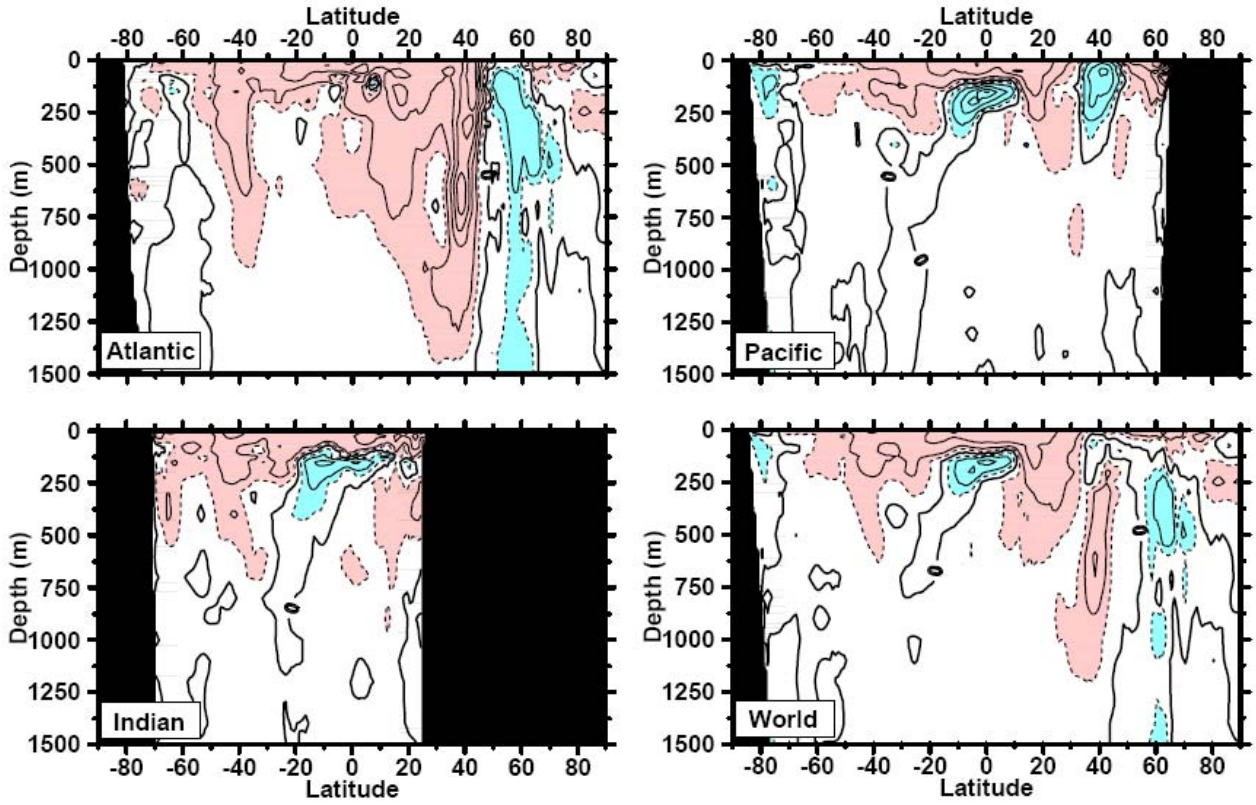

Figure 5.3. Linear trend (1955–2003) of zonally averaged temperature in the upper 1500 m of the water column of the Atlantic Ocean, Pacific Ocean, Indian Ocean, and the World Ocean. Contour interval is 0.05°C per decade. Dark, solid line is the zero contour. Red shading indicates values equal or greater than 0.025°C per decade and blue shading indicates values equal or less than –0.025°C per decade. Based on the work of Levitus et al. (2005a).

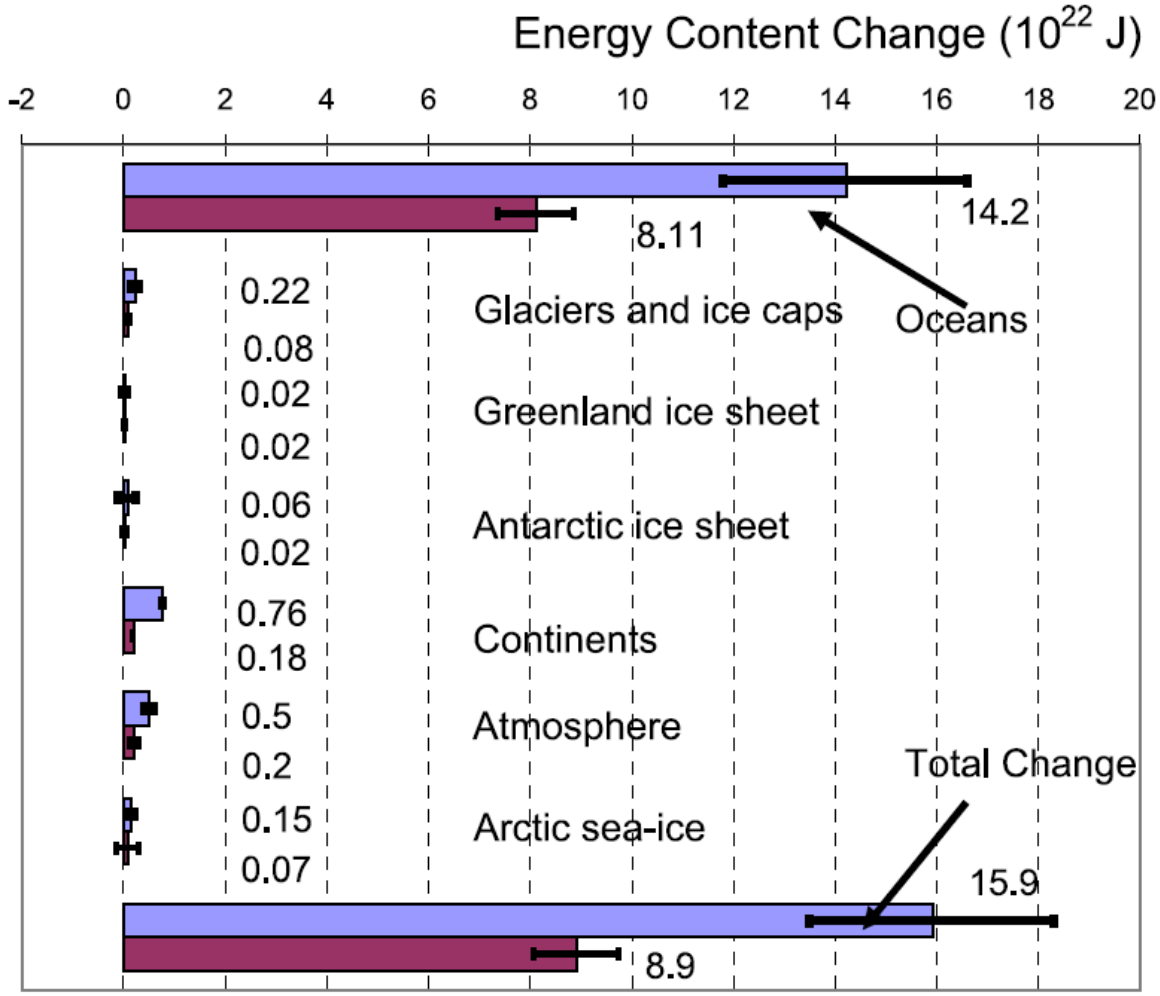

Figure 5.4. Energy content changes from different components of the Earth System for two periods (1961–2003) and (1993–2003). Blue bars are for1961–2003, burgundy 1993–2003. Ocean heat content change from this section and Levitus et al. (2005c), glaciers and ice caps, Greenland and Antarctic ice sheets from Chapter 4, continental heat content (Beltrami et al., 2002), atmospheric - energy content (e.g., Trenberth et al., 2001) and Arctic sea-ice release (Hilmer and Lemke, 2000). Positive energy content change means an increase in stored energy (i.e. heat content in oceans, latent heat from reduced ice or sea-ice volumes, heat content in the continents excluding latent heat from permafrost changes, and latent, sensible heat, potential and kinetic energy for the atmosphere). All error estimates are 90% confidence intervals. Note, no estimate of confidence is available for the continental heat gain. Some of the results have been scaled from published results for the two respective periods. Ocean heat content change for the period 1961–2003 is for the 0–3000 m layer, and for the period 1993–2003 is for 0–700 m (or 750 m) layer and is computed as an average of the trends from Ishii et al. (2006), Levitus et al. (2005a), and Willis et al. (2004).

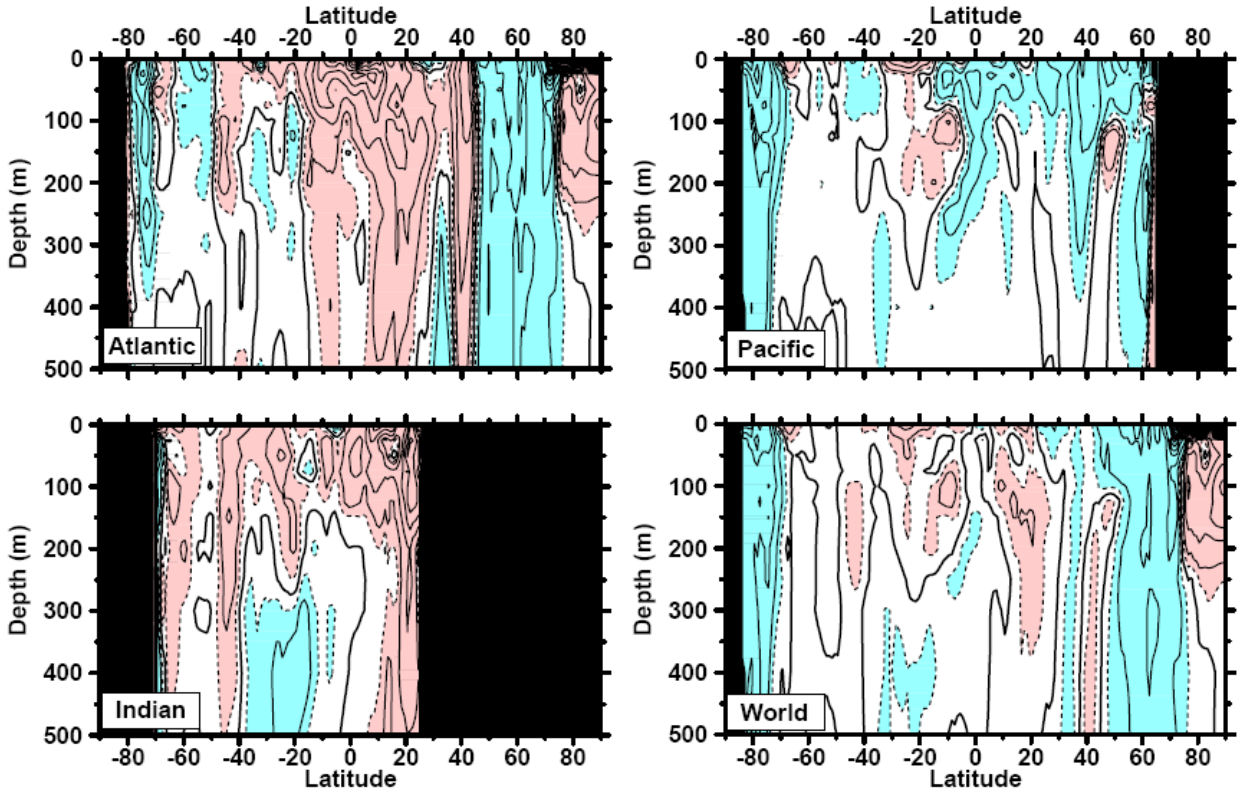

Figure 5.5: Linear trends (1955–1998) of zonally averaged salinity (Practical Salinity Scale) in the upper 500 m of the Atlantic Ocean, Pacific Ocean, Indian Ocean, and the World Ocean. Contour interval is 0.01 per decade and dashed contours are ±0.005 per decade. Dark, solid line is the zero contour. Red shading indicates values equal or greater than 0.005 per decade and blue shading indicates values equal or less than –0.005 per decade. Based on the work of Boyer et al. (2005).

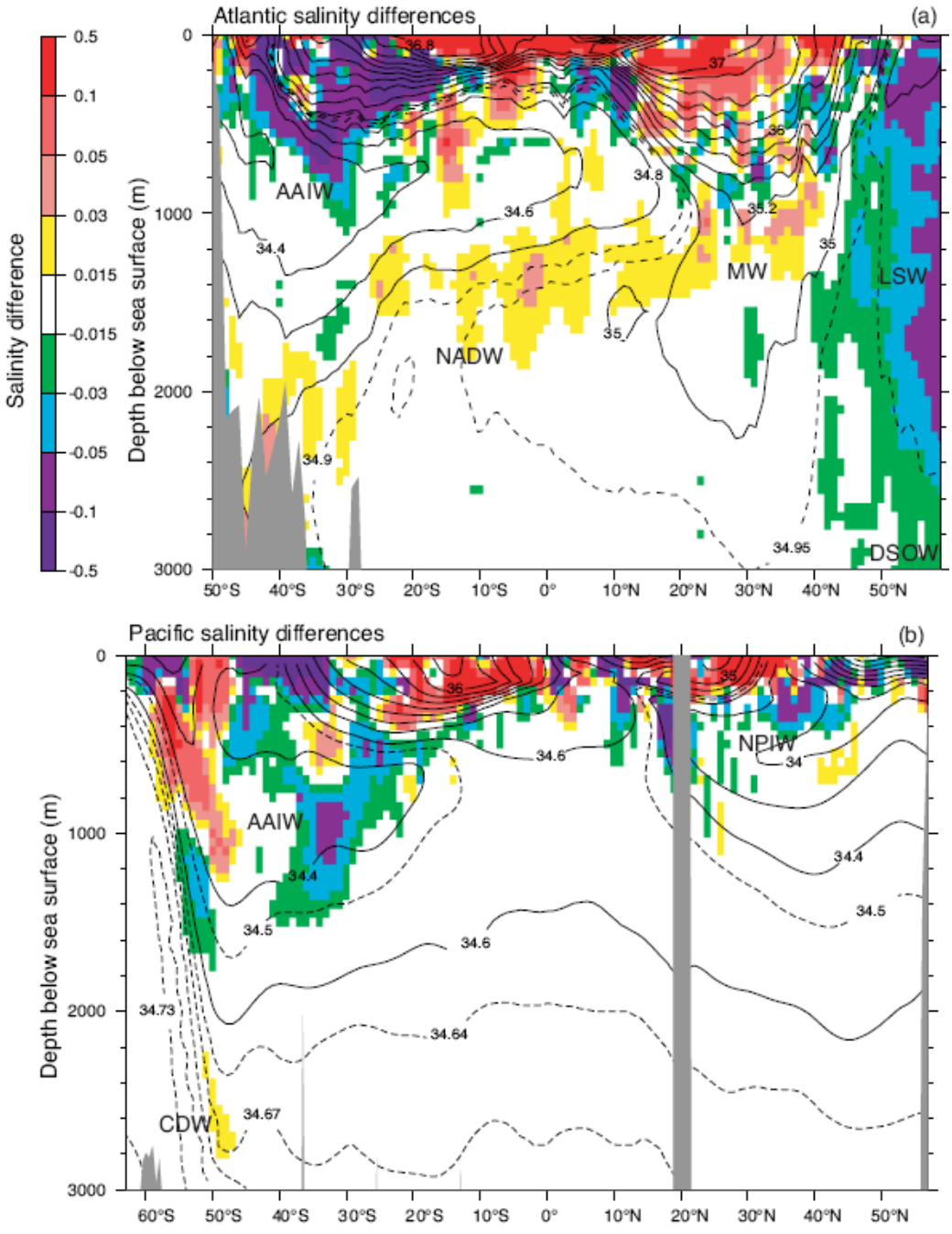

Figure 5.6. Meridional sections of differences in salinity of the a) Atlantic Ocean for the period 1985–1999 minus 1955–1969 (upper panel) and b) Pacific Ocean for the WOCE 150°W section (1991–1992) and historical data from 1968 ± 7.5 years (lower panel). Contours on these figures are the mean salinity fields along each section and show the key features. The salinity differences are difference along isopycnals that have been mapped to pressure surfaces. The Atlantic section is along the western side of the Atlantic Ocean and the Pacific section is along 150°W. The two figures are redrafted from Curry et al. (2003) and Wong et al (2001). Acronyms: AAIW (Antarctic Intermediate Water), CDW (Circumpolar Deep Water), NADW (North Atlantic Deep Water), MW (Mediterranean Water), LSW (Labrador Sea Water), DSOW (Denmark Strait Overflow Water), NPIW (North Pacific Intermediate Water).

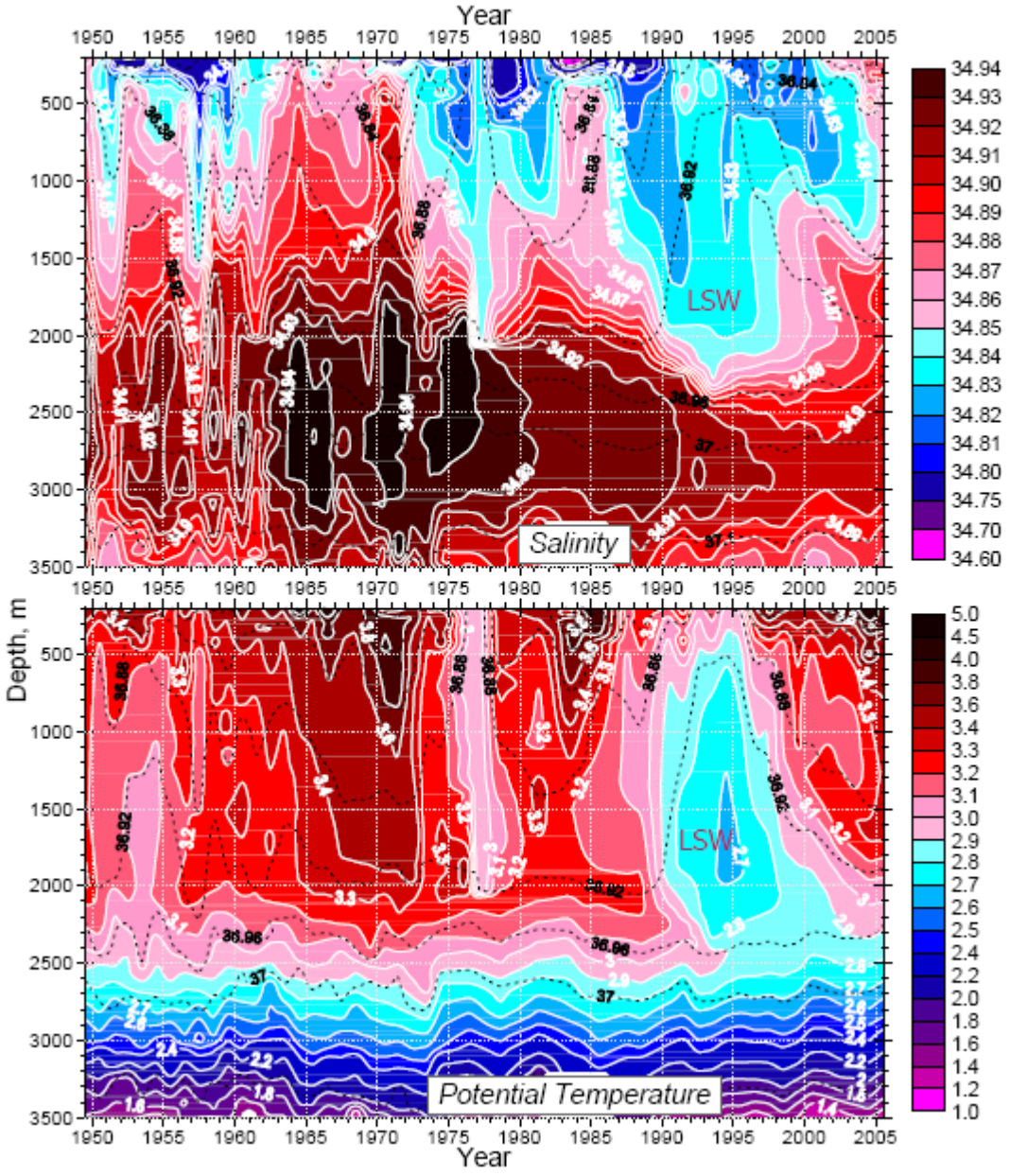

Figure 5.7. The longest available time series of a) salinity (upper panel) and b) potential temperature (lower panel) in the central Labrador Sea from 1949 to 2005 (updated from Yashayaev et al., 2003). The dashed lines are contours of potential density and are the same on both panels.

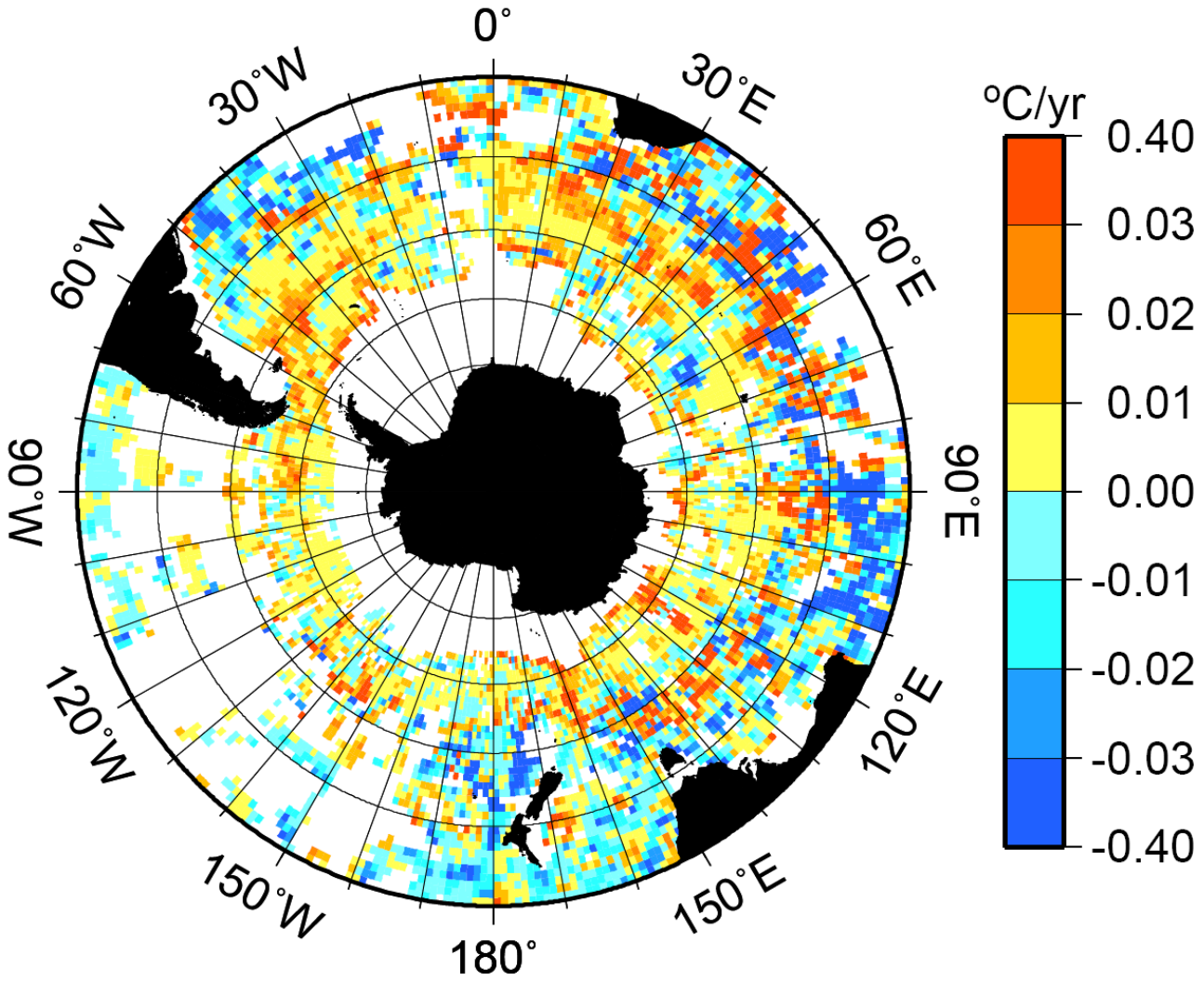

Figure 5.8. Temperature trend at 900 m depth using data collected from the 1930s to 2000, including shipboard profile and ALAS float data. The largest warming occurs in the Subantarctic, and a slight cooling to the north. From Gille (2002).

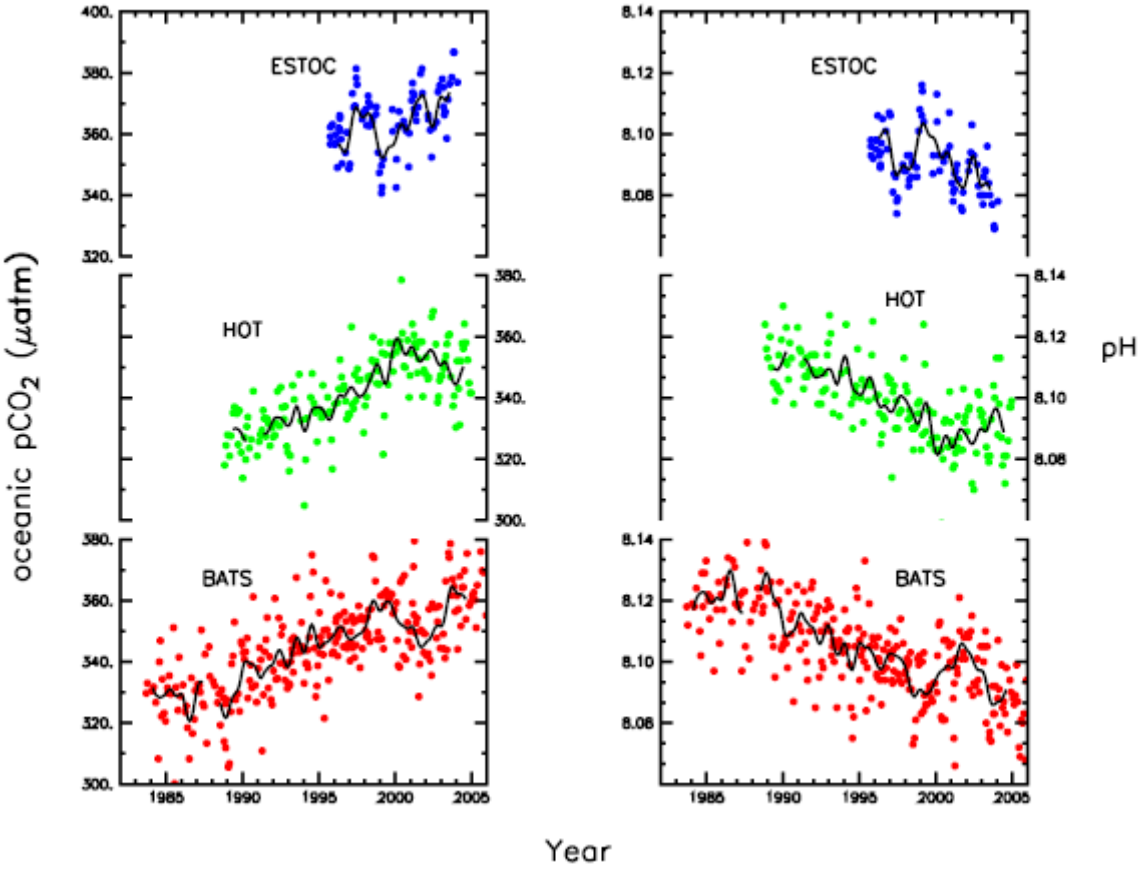

Figure 5.9. Changes in surface oceanic pCO_2 (left; in µatm) and pH (right) from three time-series stations: Blue: ESTOC (29°N, 15°W; Gonzalez-Dávila et al., 2003). Green: HOT (23°N, 158°W; Dore et al., 2003). Red; BATS (31/32°N, 64°W; Bates et al., 2002; Gruber et al., 2002). pCO_2 and pH were calculated from Dissolved Inorganic Carbon and alkalinity at HOT and BATS. pH was directly measured at ESTOC and pCO_2 was calculated from pH and alkalinity. The mean seasonal cycle was removed from all data. The thick black line filters variability less than 0.5 years.

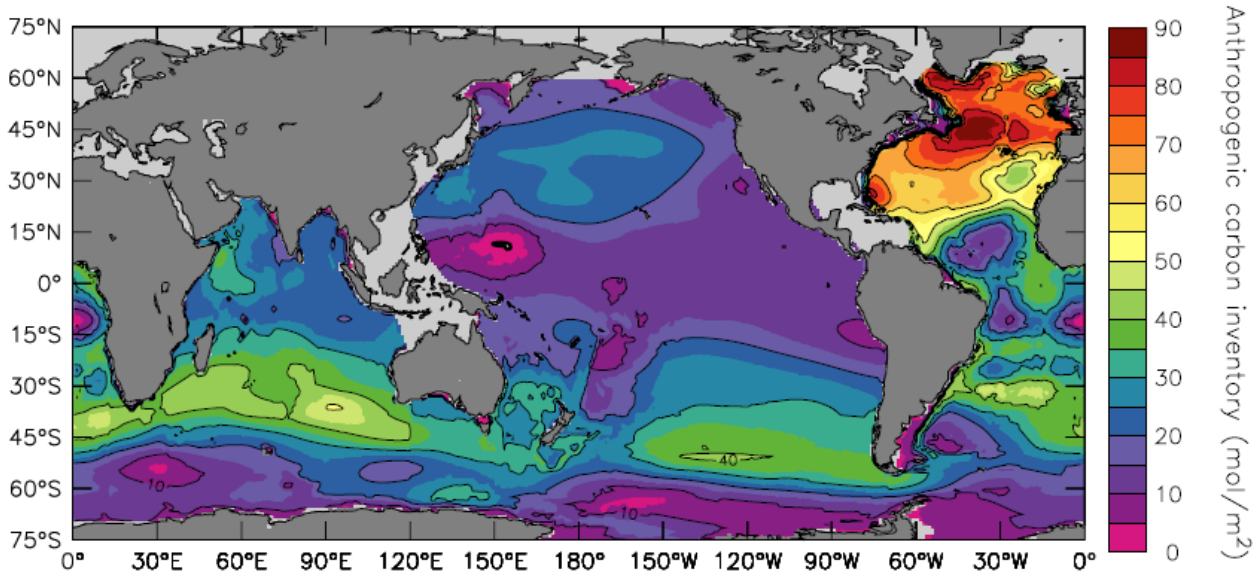

Figure 5.10. Column inventory of anthropogenic carbon (mol /m^2) as of year 1994 from (Sabine et al., 2004a). Anthropogenic carbon is estimated indirectly by correcting the measured Dissolved Inorganic Carbon (DIC) for the contributions of organic matter decomposition and dissolution of carbonate minerals, and taking into account the DIC concentration the water had in the pre-industrial ocean when it was last in contact with the atmosphere. The global inventory of anthropogenic carbon taken up by the ocean between 1750 and 1994 is estimated to be 118 ± 19 Gt C.

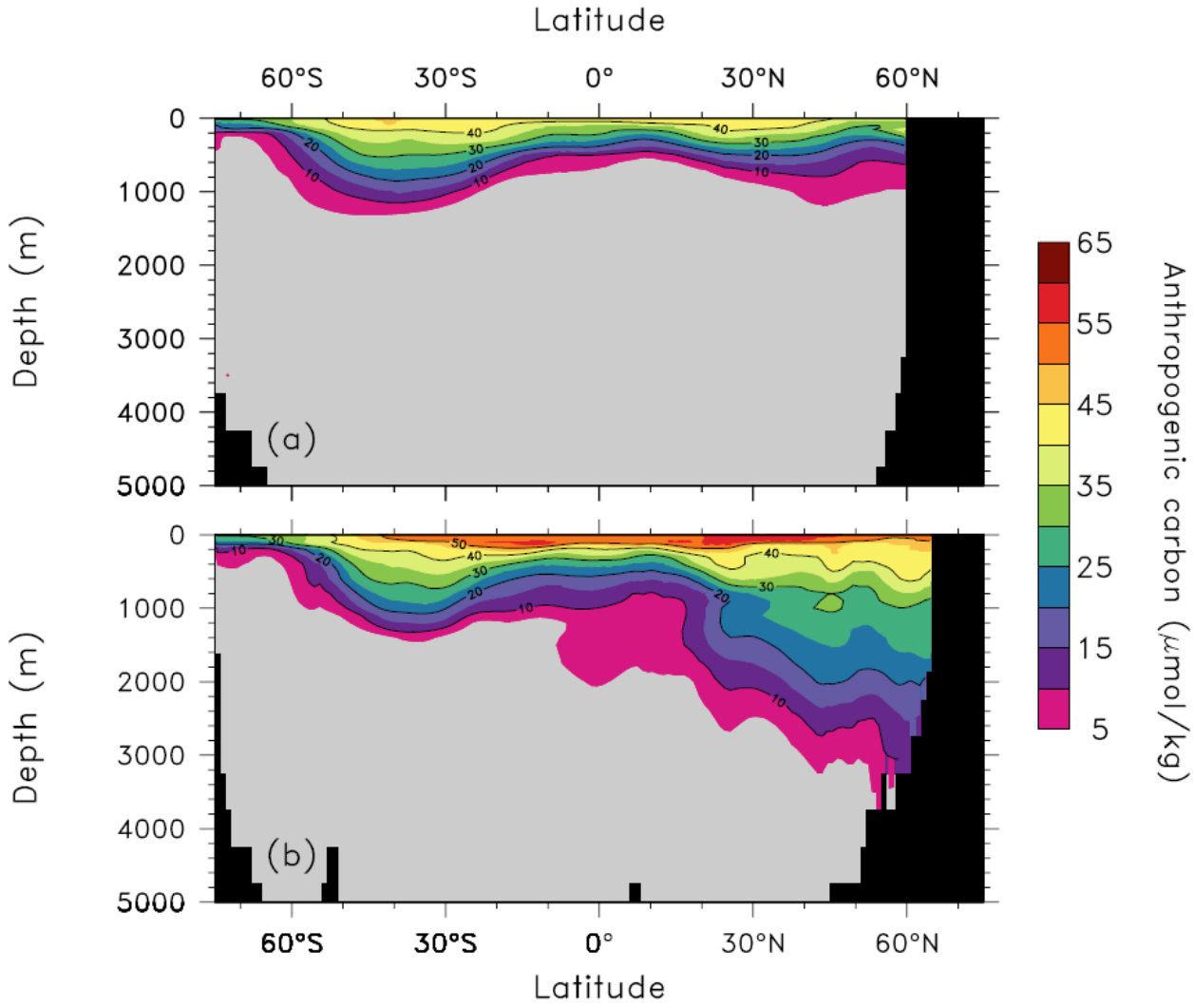

Figure 5.11. Mean concentration of anthropogenic carbon as of year 1994 in µmol/kg from (Sabine et al., 2004a) averaged over the Pacific and Indian Oceans (a) and the Atlantic Ocean (b). The calculation of anthropogenic carbon is described in the caption of Figure 5.10 and in the text (Section 5.4).

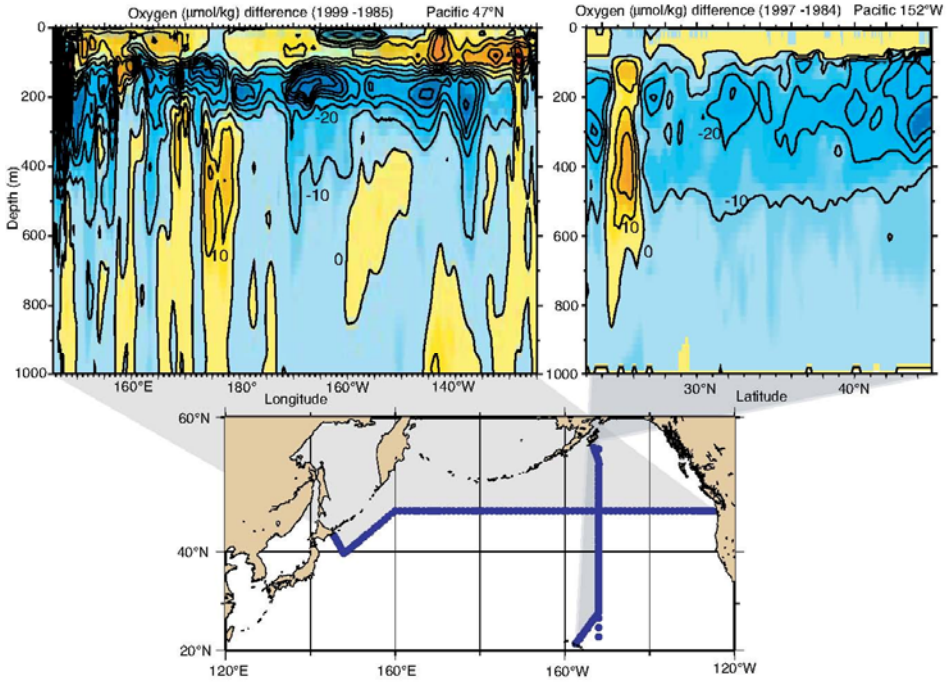

Figure 5.12. Changes in oxygen concentration (µmol/kg) along two sections in the North Pacific (see map, bottom panel). Top left panel: Difference 1999 minus 1985 along 47°N. Top right panel: Difference 1997 minus 1984 at 152°W. Blue colors indicate decrease, yellow colors increase of oxygen over time. The differences were calculated using density as the vertical coordinate. After Deutsch et al. (2005).

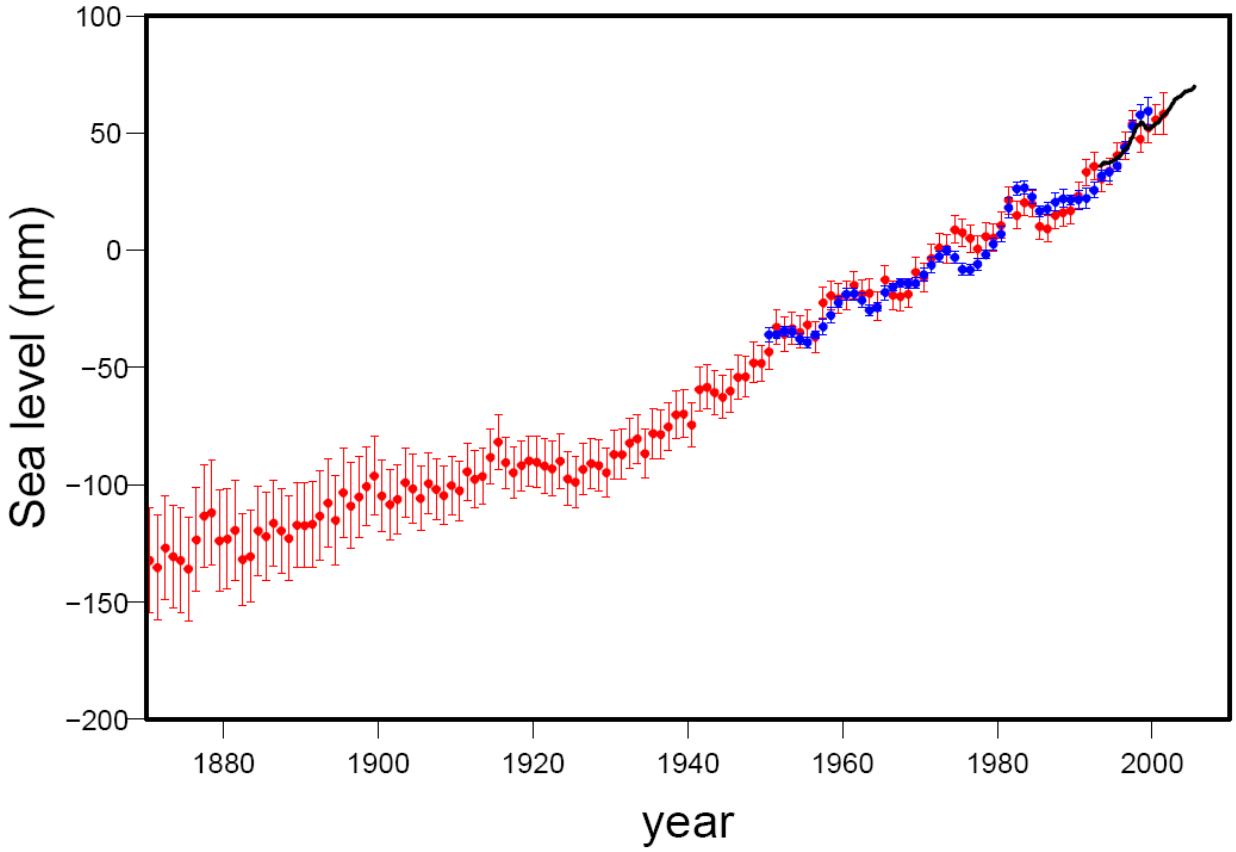

Figure 5.13. Annual averages of the global mean sea level. Red curve: Reconstructed sea level fields since 1870 (updated from Church and White, 2006). Blue curve: Coastal tide gauges measurements since 1950 (from Holgate and Woodworth, 2004). Black curve: Based on satellite altimetry (Leuliette et al., 2004). Units are in mm. The red and blue curves are deviation from their average 1961–1990, and the shorter black curve is the deviation from the average of the red curve for the period 1993–2001. Error bars are 90% confidence intervals.

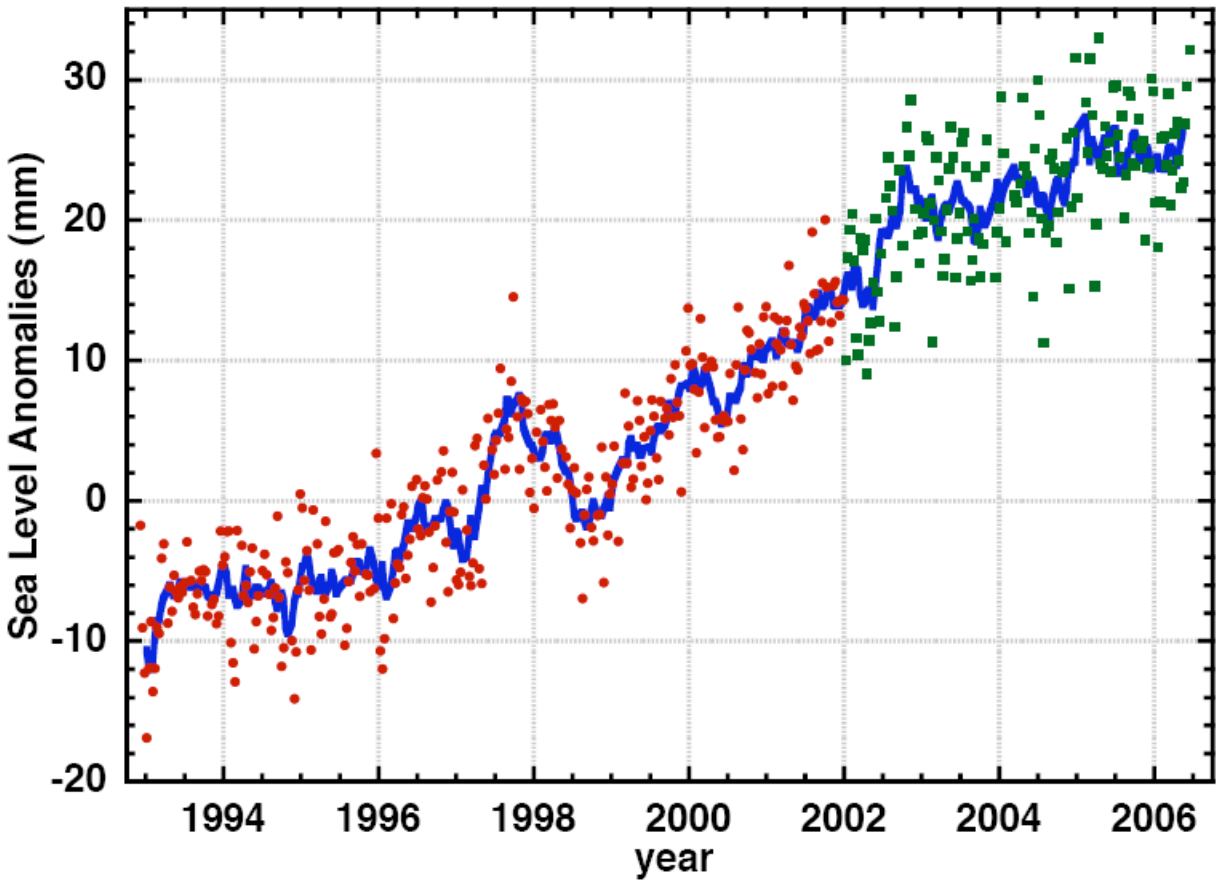

Figure 5.14. Variations in global mean sea level computed from satellite altimetry from January 1993 to October 2005, averaged over 65°S–65°N. Dots are 10-day estimates (from Topex/Poseidon satellite in red and Jason in green). The blue solid curve corresponds to 60-day smoothing. Updated from Cazenave and Nerem (2004) and Leuliette et al. (2004).

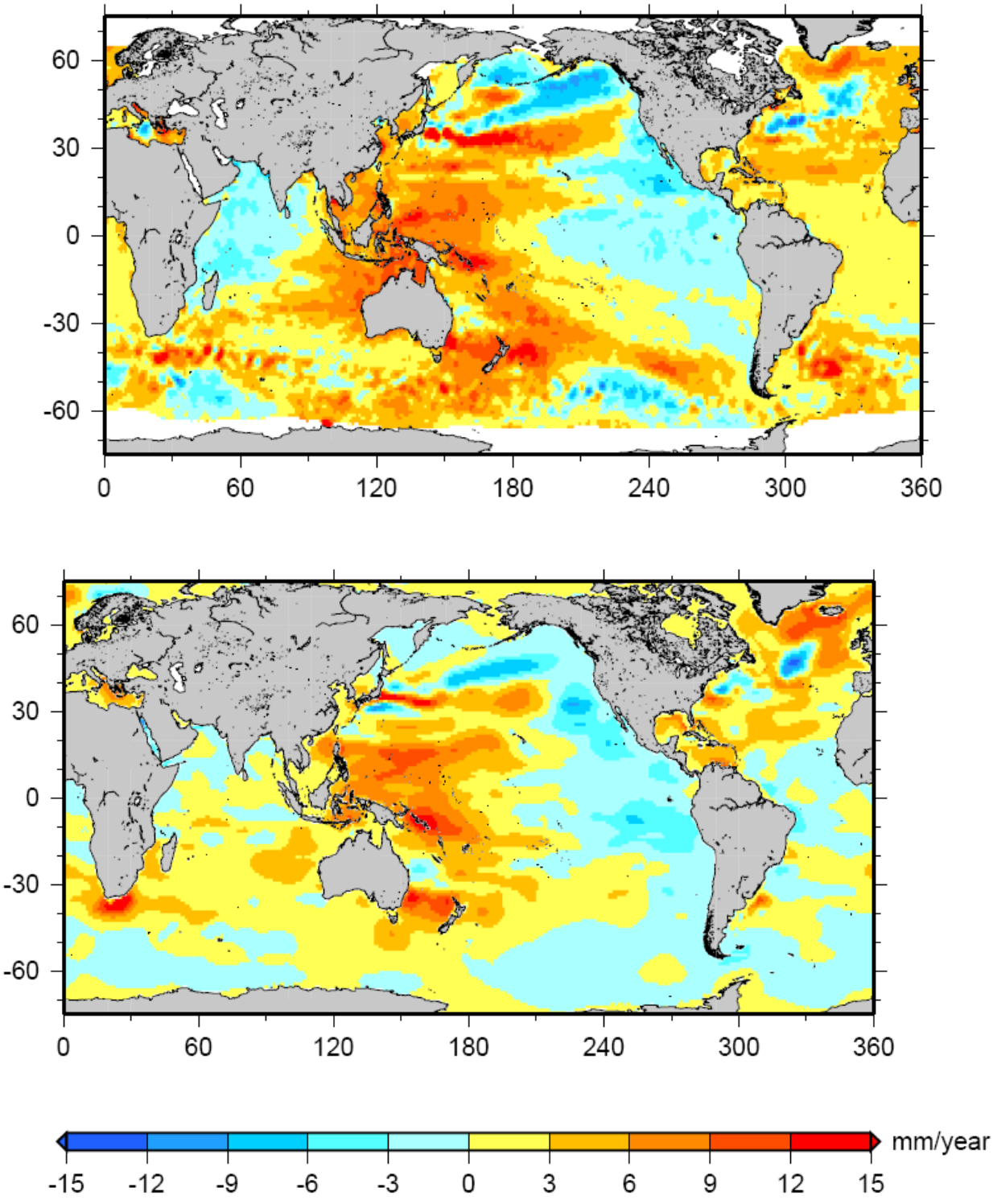

Figure 5.15. (a) Geographic distribution of short term linear trends in mean sea level for 1993–2003 based on Topex/Poseidon satellite altimetry (updated from Cazenave and Nerem, 2004), and (b) geographic distribution of linear trends in thermal expansion for 1993–2003 (based on temperature data from Ishii et al., 2006, down to 700 m). Units are in mm/yr.

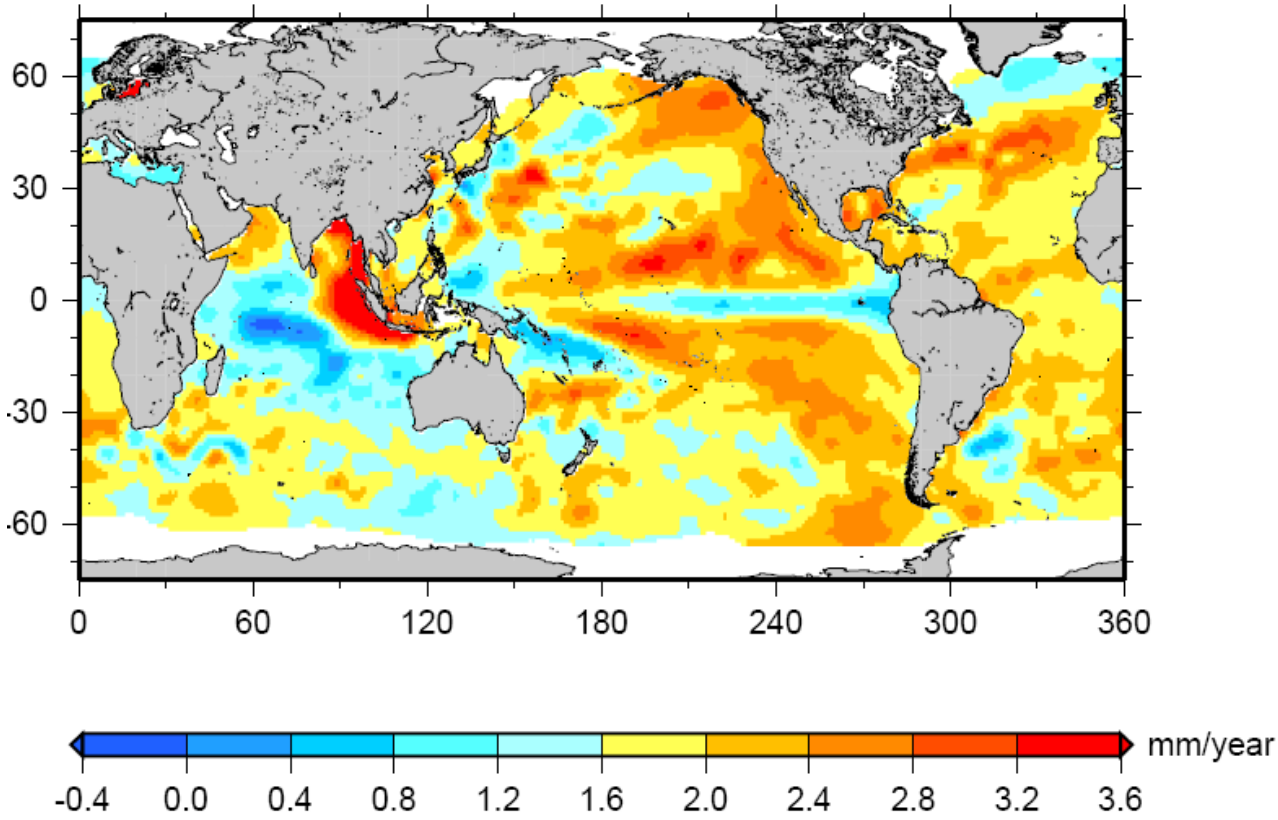

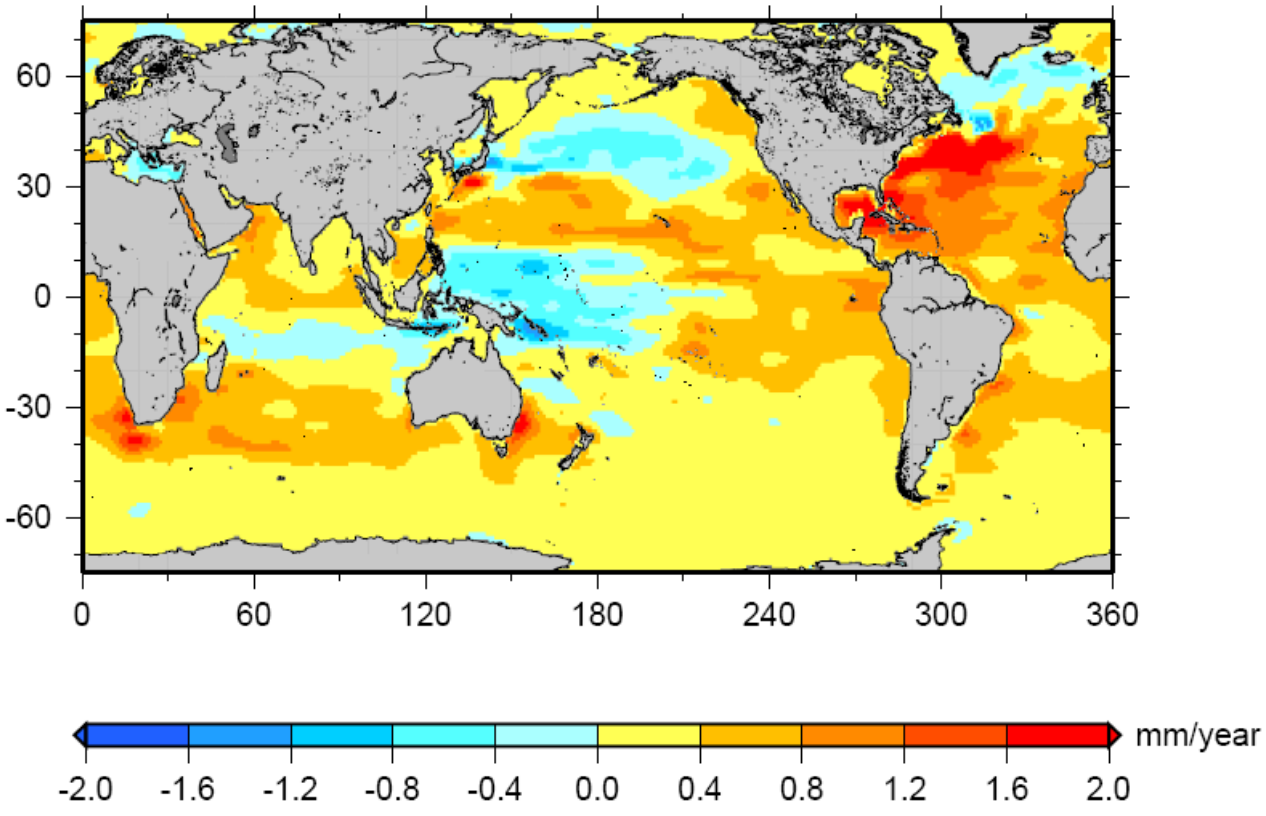

Figure 5.16. (a) Geographic distribution of long term linear trends in mean sea level for 1955–2003 based on the past sea level reconstruction with tide gauges and altimetry data (updated from Church et al., 2004), and (b) geographic distribution of linear trends in thermal expansion for 1955–2003 (based on temperature data

from Ishii et al., 2006, down to 700 m). Units are in mm/yr. Note that colors in the upper figure denote 1.6 mm yr^{-1} higher values.

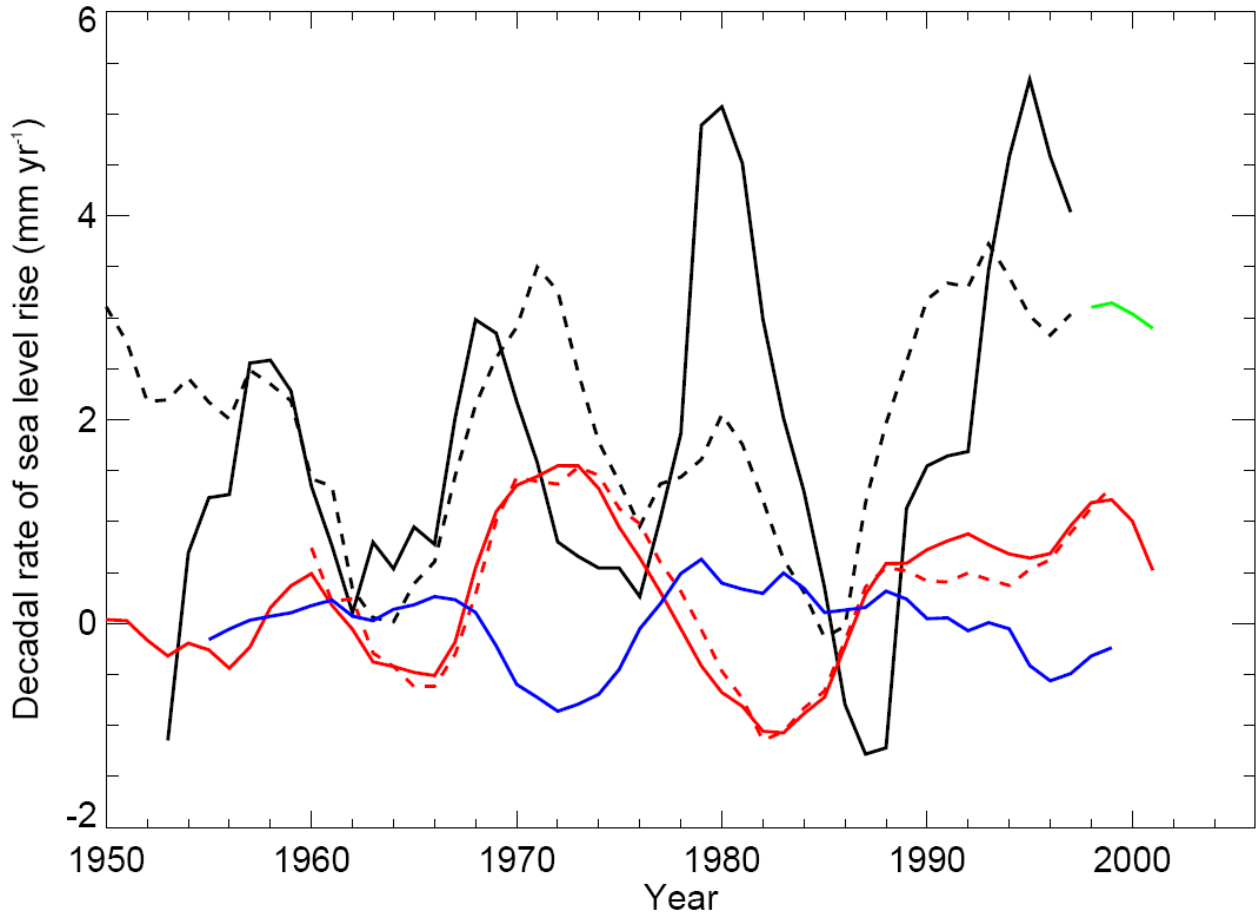

Figure 5.17. Overlapping 10-year rates of global sea level change from tide-gauge datasets (Holgate and Woodworth, 2004, in solid black; Church and White, 2006, in dashed black) and satellite altimetry (updated from Cazenave and Nerem, 2004, in green), and contributions to global sea level change from thermal expansion (Ishii et al, 2006, in solid red; Antonov et al, 2005, in dashed red) and climate-driven land water storage (Ngo-duc et al, 2005, in blue). Each rate is plotted against the middle of its 10-year period.

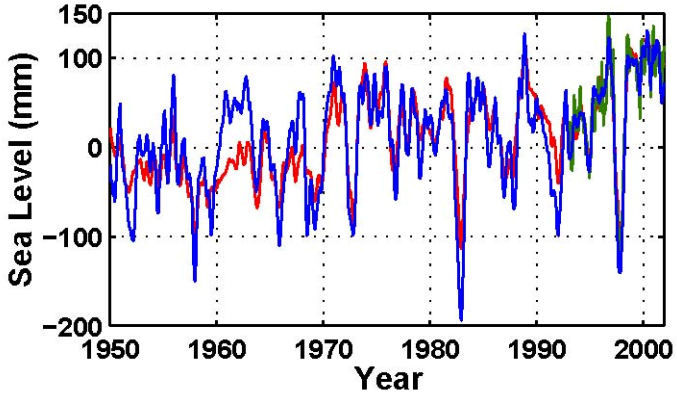

Figure 5.18. Monthly mean sea level curve for 1950–2000 at Kwajalein (8°44'N, 167°44'E). The observed sea level (from tide gauge measurements) is in blue, the reconstructed sea level in red, and the satellite altimetry record in green. Annual and semi-annual signals are removed from each time series and the tide gauge data has been smoothed. The figure was drawn using techniques in Church et al. (2004) and Church and White (2006).

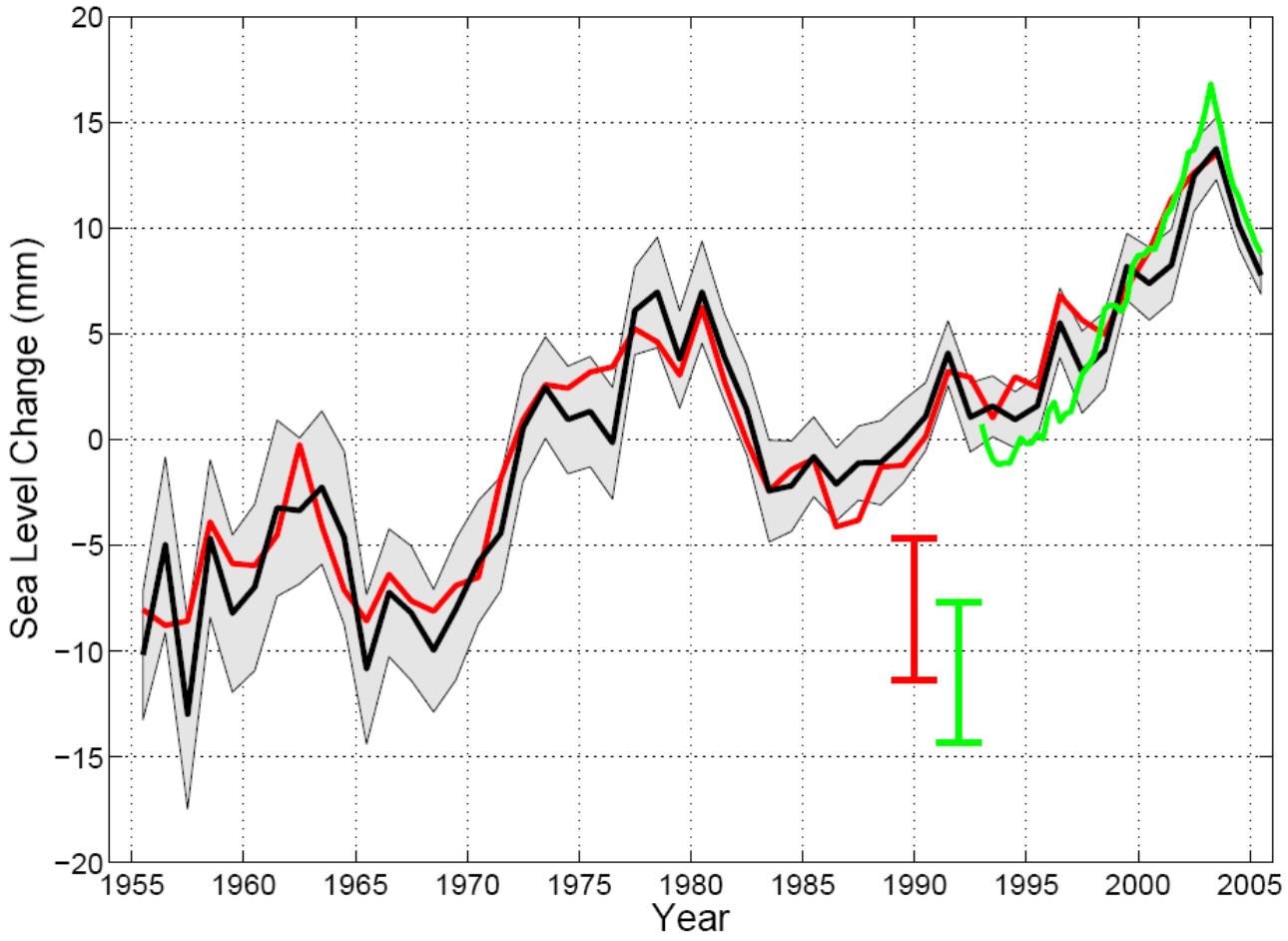

Figure 5.19. Global sea level change due to thermal expansion for 1955–2003, based on Levitus et al. (2005a) (black line) and Ishii et al. (2006) (red line), for 1955–2003, 0–700 m layer, and for upper 750 m by Willis et al. (2004) (green line). The shaded area and the vertical red and green error bars represent the 90% confidence interval. The black and red curves denote the deviation from their 1961–1990 average, the shorter green curve the deviation from the average of the black curve for the period 1993–2003.

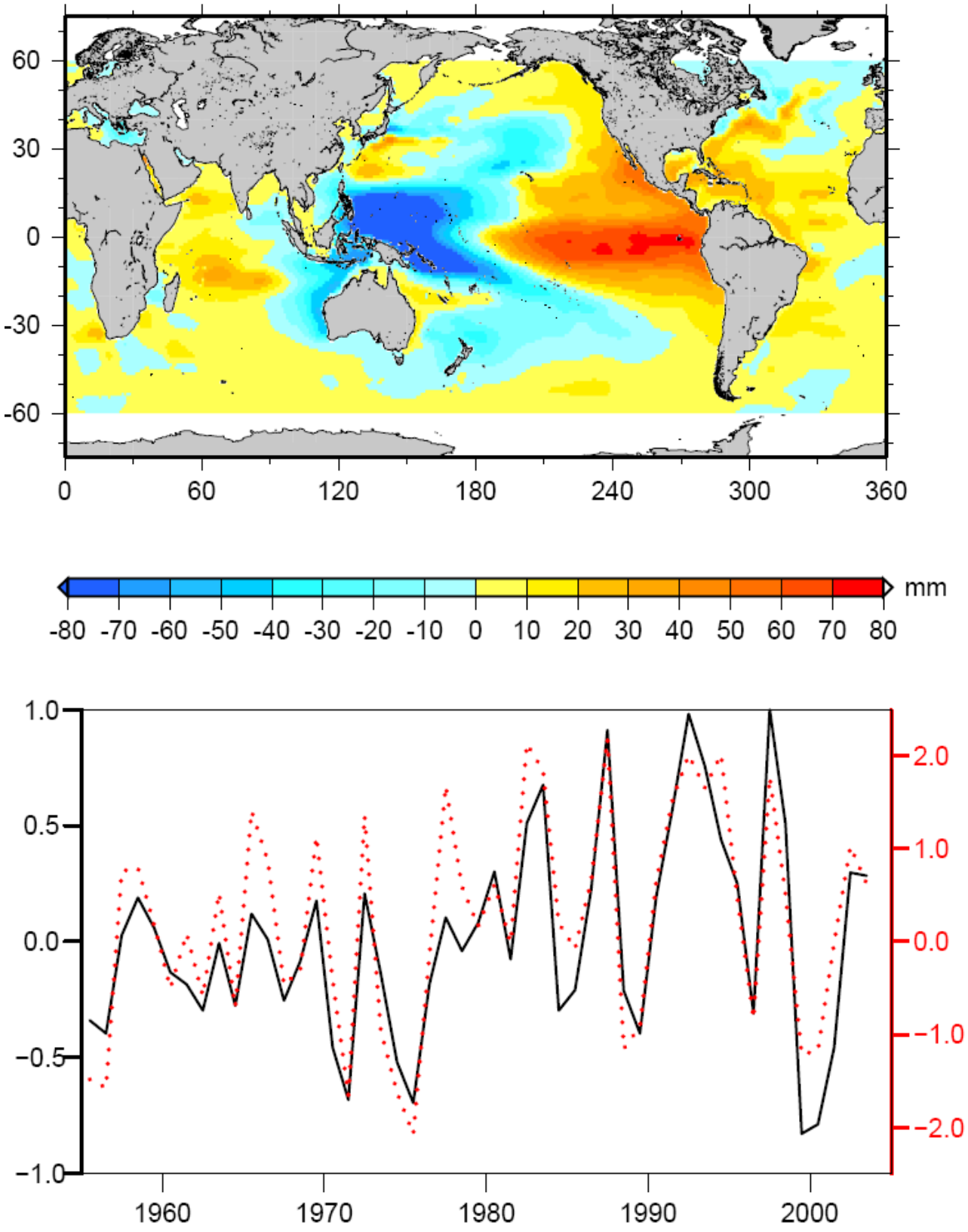

Figure 5.20. (a) First mode of the EOF decomposition of the gridded thermosteric sea level time series of yearly temperature data down to 700 m from Ishii et al. (2006). (b) The normalized principal component (black solid curve) is highly correlated with the negative southern oscillation index (dotted red curve).

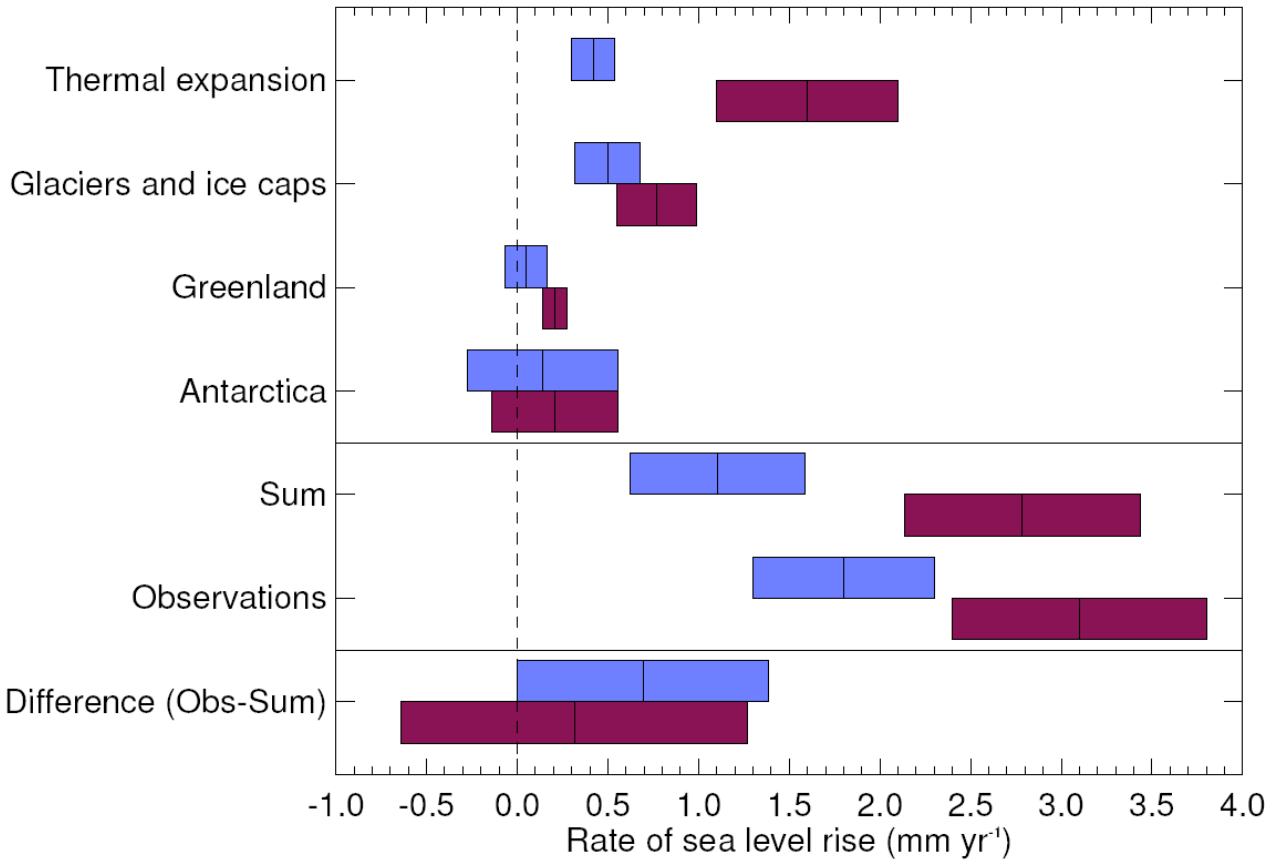

Figure 5.21. Estimates of the various contributions to the budget of the global mean sea level change (upper four entries), the sum of these contributions and the observed rate of rise (middle two), and the difference observed rate minus sum of contributions (lower), all for 1961–2003 (blue) and 1993–2003 (red). The bars represent 90% error range. The errors of the separate terms have been combined in quadrature to obtain the error on their sum. Likewise the errors of the sum and the observed rate have been combined in quadrature to obtain the error for the difference.

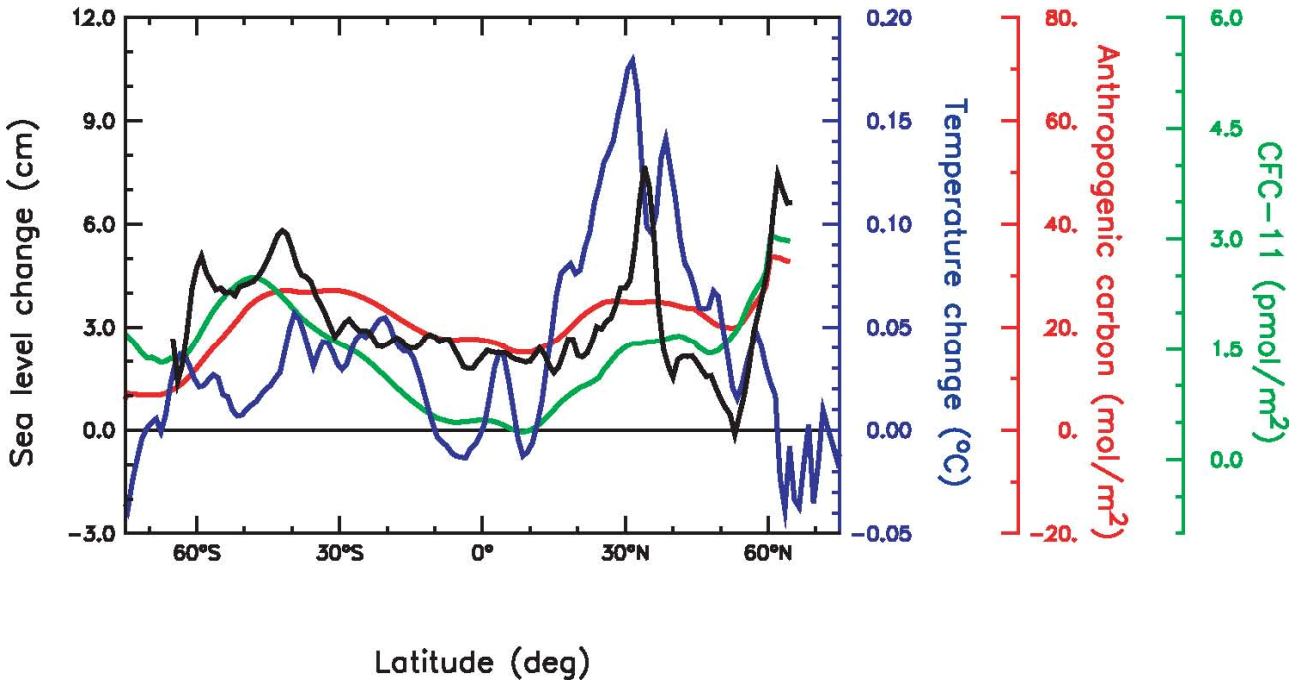

Figure 5.22. Averages of temperature change (blue, from Levitus et al., 2005a), anthropogenic carbon (red, from Sabine et al., 2004a) and CFC-11 (green, from Willey et al., 2004) along lines of constant latitude over the top 700 m thick layer of the upper ocean. Also shown is sea-level change averaged along lines of constant latitude (black, from Cazenave and Nerem, 2004). The temperature changes are for the 1955–2003 period, the anthropogenic carbon is since pre-industrial times (i.e., 1750), CFC-11 concentrations are for the period 1930 to 1994, and sea-level for the period 1993 to 2003.

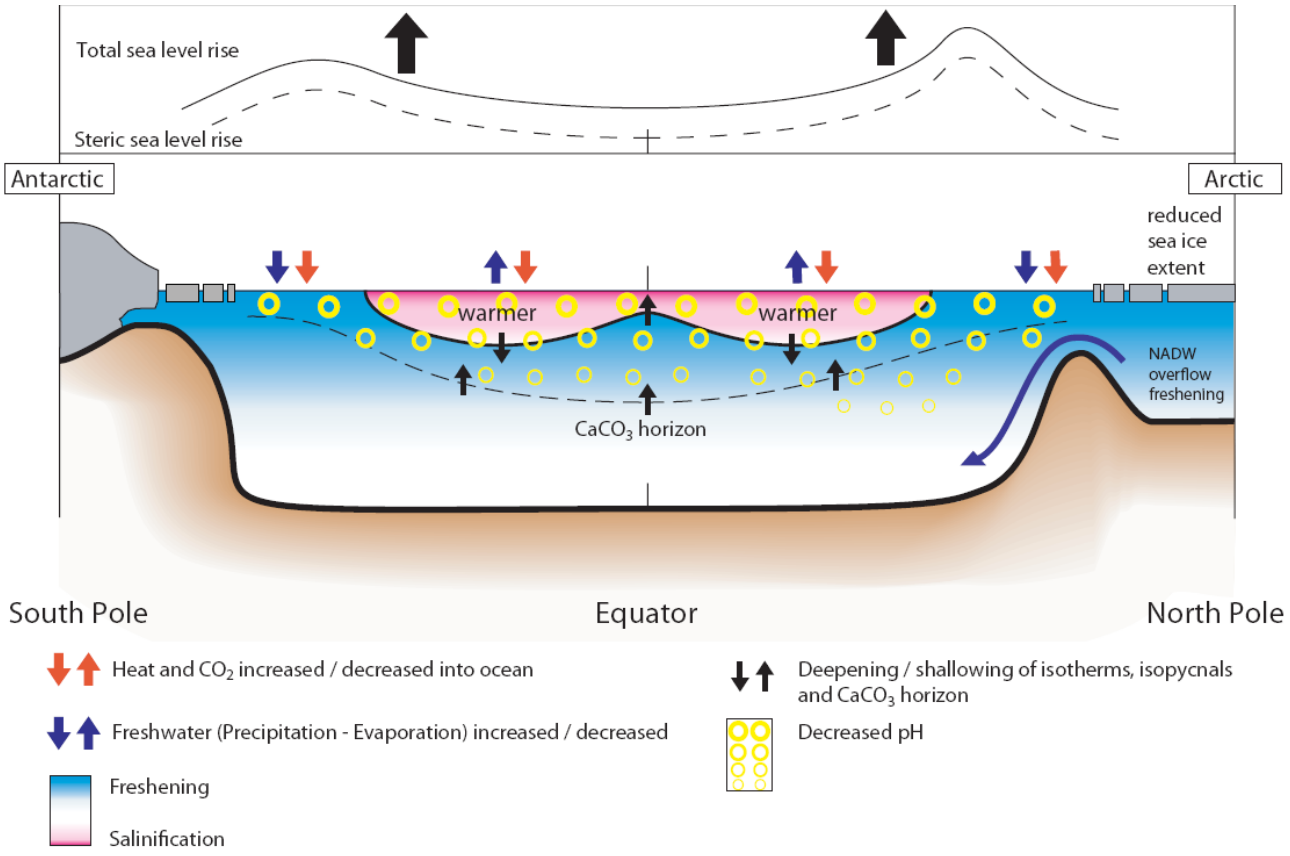

Figure 5.23. Schematic of the observed changes in the ocean state, including ocean temperature, ocean salinity, sea-level, sea-ice and bio-geochemical cycles. The legend identifies the direction of the changes in these variables.

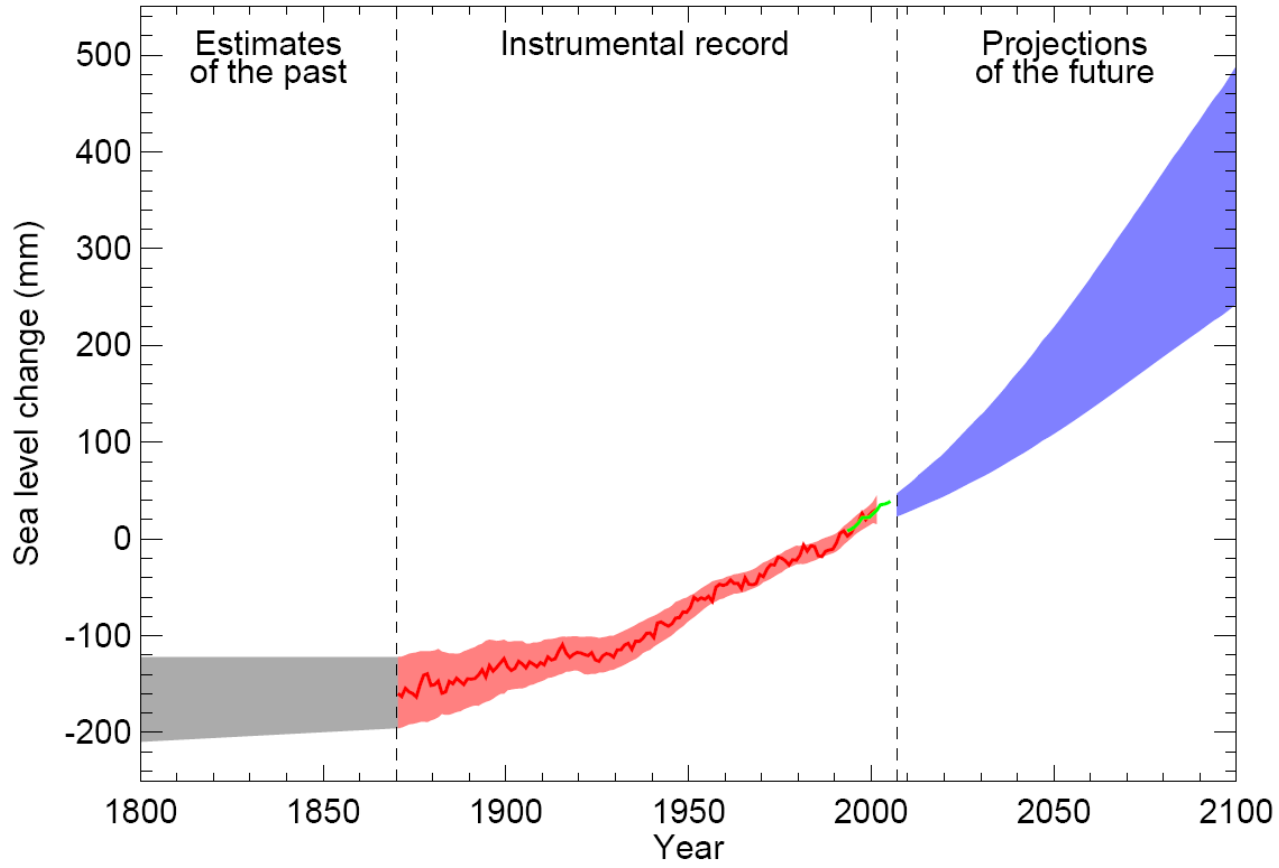

FAQ 5.1, Figure 1. Time-series of global mean sea level in the past and as projected for the future. For the period before 1870, we do not have global measurements of sea level. The grey shading shows the uncertainty on the estimated long-term rate of sea level change (Chapter 6, Section 6.4.3). The red line is a reconstruction of global-mean sea level from tide gauges (Section 5.5.2.1), and the red shading denotes the range of variations from a smooth curve. The zero on the y-axis is chosen such that the period 1980–1999 has a zero mean. The green line is global mean sea level observed from satellite altimetry. The blue shading is the range of model projections for the SRES A1B scenario for the 21st century, relative to the 1980–1999 mean, and has been calculated independently from the observations. Beyond 2100 the projections are increasingly dependent on the scenario. See Chapter 10 for a discussion of sea level rise projections for other scenarios considered in this report. Over many centuries or millennia, sea level could rise by several metres (Chapter 10, Section 10.7.4).

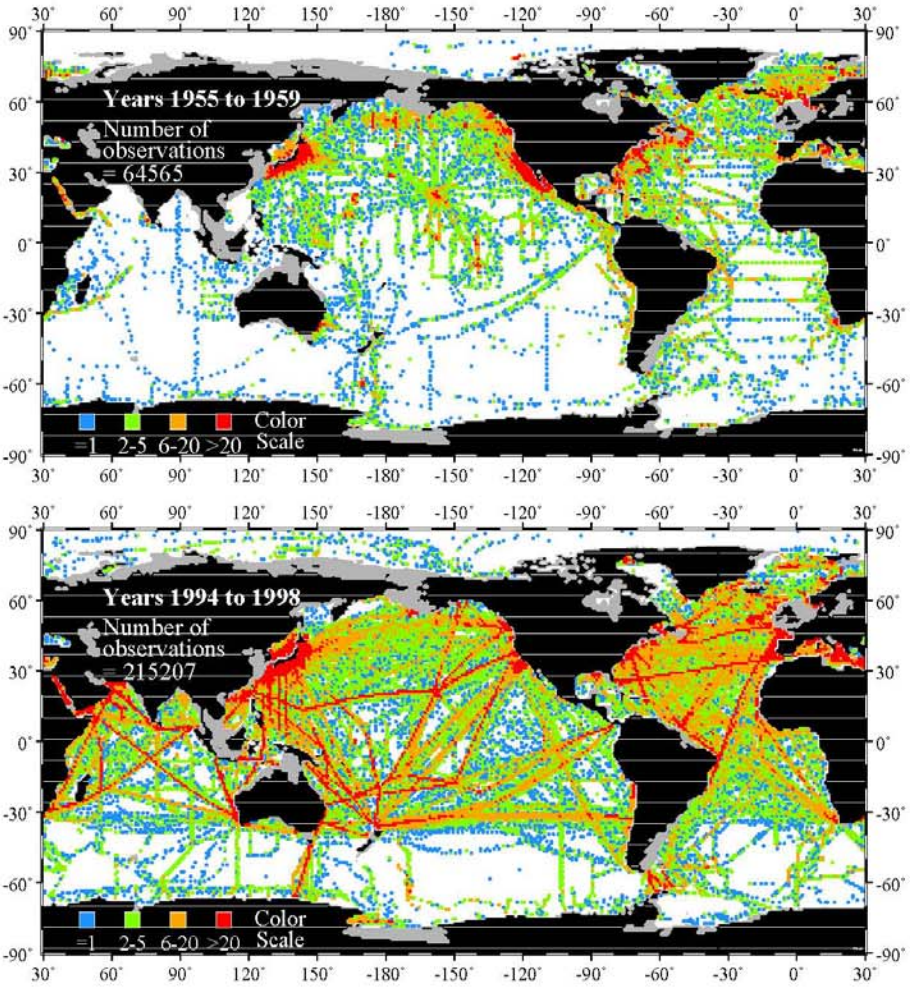

Figure 5.24. Number of ocean temperature observations in each 1-degree grid box at 250 m depth for two periods, one with low and one with high density of observations. Upper figure: years 1955–1959 (a), lower figure: years 1994–1998 (b). A blue dot indicates a 1-degree grid box containing 1 observation, green dot 2–5 observations, orange dot 6–20 observations, and a red dot greater than 20 observations.

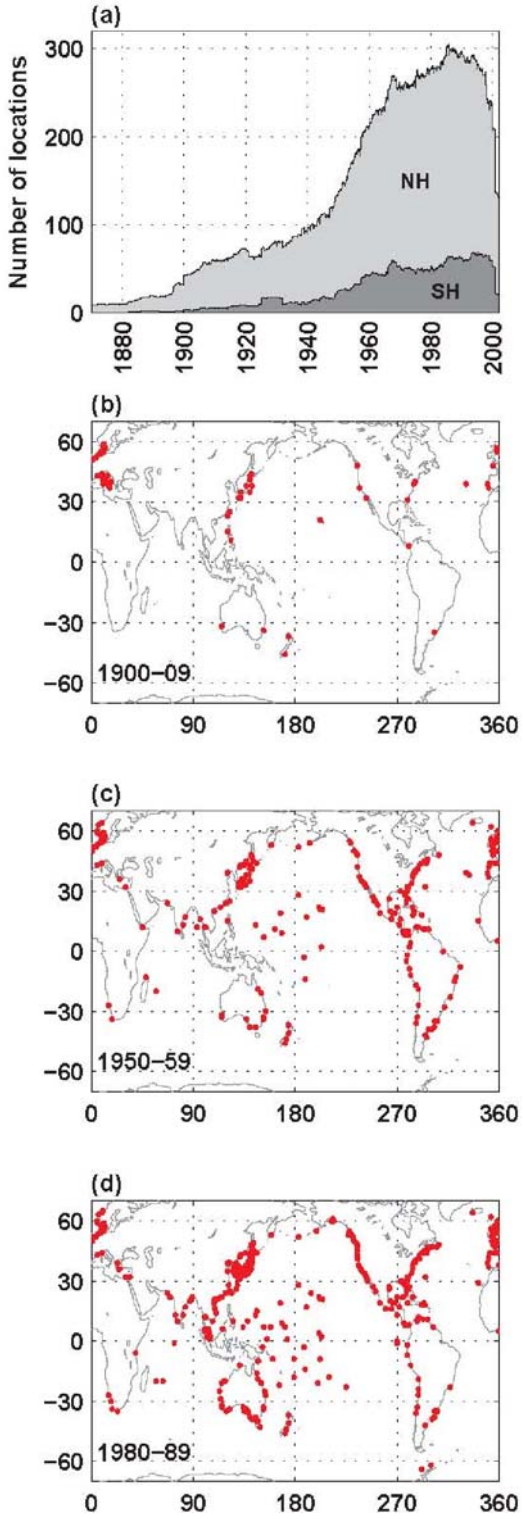

Figure 5.25. (a) Number of tide gauge stations in Northern Hemisphere (NH) and Southern Hemisphere (SH) used to derive the global sea level curve (red and blue curves in Figure 5.13), as a function of time. (b) – (d): Spatial distribution of tide gauge stations (denoted by red dots) for the periods 1900–1909 (b), 1950–1959 (c) and 1980–1998 (d).